ACS OMEGA

http://pubs.acs.org/journal/acsodf

Article

Hybrid Surface-Enhanced Raman Scattering Substrates for the Trace Detection of Ammonium Nitrate, Thiram, and Nile Blue

Jagannath Rathod, Chandu Byram, Ravi Kumar Kanaka, Moram Sree Satya Bharati, Dipanjan Banerjee, Mangababu Akkanaboina, and Venugopal Rao Soma*

Cite This: *ACS Omega* 2022, 7, 15969−15981

Read Online

ACCESS | Metrics & More | Article Recommendations | Supporting Information

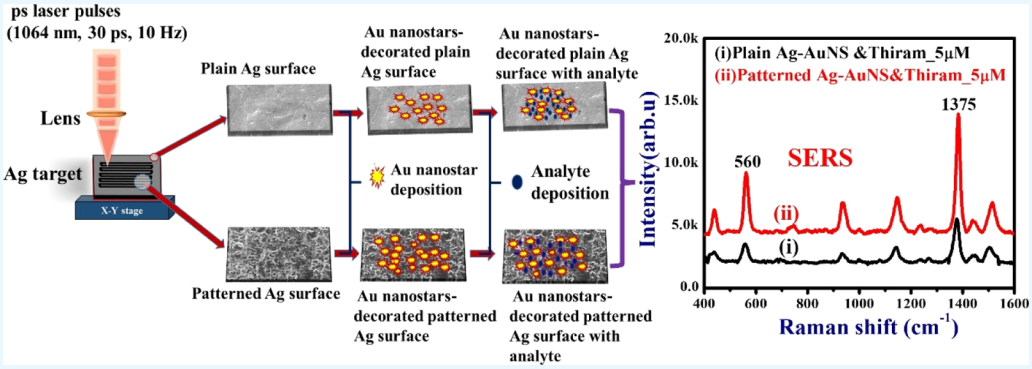

ABSTRACT: We report the fabrication and performance evaluation of hybrid surface-enhanced Raman scattering (SERS) substrates involving laser ablation and chemical routes for the trace-level detection of various analyte molecules. Initially, picosecond laser ablation experiments under ambient conditions were performed on pure silver (Ag) and gold (Au) substrates to achieve distinct nanosized features on the surface. The properties of the generated surface features on laser-processed portions of Ag/Au targets were systematically analyzed using UV−visible reflection and field emission scanning electron microscopy studies. Later, hybrid-SERS substrates were achieved by grafting the chemically synthesized Au nanostars on the plain and laser-processed plasmonic targets. Subsequently, we employed these as SERS platforms for the detection of a pesticide (thiram), a molecule used in explosive compositions [ammonium nitrate (AN)], and a dye molecule [Nile blue (NB)]. A comparative SERS study between the Au nanostar-decorated bare glass, silicon, Ag, Au, and laser-processed Ag and Au targets has been established. Our studies and the obtained data have unambiguously determined that laser-processed Ag structures have demonstrated reasonably good enhancements in the Raman signal intensities for distinct analytes among other substrates. Importantly, the fabricated hybrid SERS substrate of "Au nanostar-decorated laser-processed Ag" exhibited up to eight times enhancement in the SERS intensity compared to laser-processed Ag (without nanostars), as well as up to three times enhancement than the Au nanostar-loaded plain Ag substrates. Additionally, the achieved detection limits from the Au nanostar-decorated laser-processed Ag SERS substrate were ∼50 pM, ∼5 nM, and ∼5 μM for NB, thiram, and AN, respectively. The estimated enhancement factors accomplished from the Au nanostar-decorated laser-processed Ag substrate were ∼10^6, ∼10^6, and ∼10^4 for NB, thiram, and AN, respectively.

INTRODUCTION

Gold (Au) nanomaterials are the maximum studied nanotechnological tools in diverse fields including surface-enhanced Raman spectroscopy (SERS), catalysis, biosensing, and bioimaging due to easy synthesis methods, chemical stability, biocompatibility, and outstanding optical properties.[1−4] Particularly, the localized surface plasmonic resonance (SPR) property of Au nanomaterials can be tuned from the visible to near-infrared region depending on the morphology with respect to the size and shape.[5−7] In the recent years, Au nanostars have stimulated enormous attention in the fabrication of SERS substrates because of the induced high electric fields at their sharp tips, unlike their spherical, triangular, and nanorod counterparts.[8−10] In most of the previous studies, chemically synthesized nanoparticles (NPs) with different shapes were embedded on different substrates, such as glass, silicon, paper(s), fabrics, and so forth, for being used as SERS sensors for the detection of distinct analyte molecules.[6,11−14] Recently, a few novel strategies have been

Received: February 23, 2022
Accepted: April 18, 2022
Published: April 28, 2022

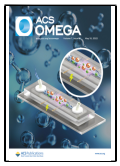

https://doi.org/10.1021/acsomega.2c01095
ACS Omega 2022, 7, 15969−15981

demonstrated for patterned SERS substrates coated with NPs of various shapes for the detection of diverse analytes.[15−18] The patterned substrates along with NPs with diverse shapes have demonstrated a significant improvement in the detection sensitivity due to the embedded NPs, along with the patterned areas acting as hotspot regions and increasing the SPR strength, resulting in strong electric fields at the confined regions.[18−20] Abundant fabrication procedures have been established for fabricating patterned substrates on countless materials, among which short/ultrashort laser ablation is a simple, fast, and efficient fabrication tool for the generation of distinct surface structures on various substrates.[21−26] Since the past 2 decades, substantial improvements have been made in achieving diverse nanostructures (NSs) on a wide range of materials such as metals, semiconductors, insulators, and polymers by varying the short/ultrashort laser ablation parameters (pulse duration, wavelength, fluence, number of pulses, and focusing conditions) and surrounding environments (air, gas, and liquid).[21,25,27−34] The ultrashort laser-induced surface structures have proven to be promising candidates in diverse areas such as sensing,[22,35−39] surface wetting (hydrophobicity and hydrophilicity),[27] electrochemistry,[40,41] and plasmonics.[27,41] Moram et al. have detected several explosive molecules using silicon (Si) microsquared arrays embedded with Ag/Au NP SERS substrates achieved using femtosecond (fs) laser ablation.[37] In a few of our earlier reports,[42,43] we have reported the utility of Au film-coated Fe/Ni NSs achieved by fs laser irradiation in different liquids for the detection of explosives and pesticides. In another study, we also demonstrated the fabrication of Au NP and nanostars using laser ablation and wet chemical approaches and further examined the SERS performance by integrating them with bare Si/filter paper. In these studies, superior SERS enhancements were observed for Au nanostar-decorated substrates as compared to the spherical Au NP-based substrates.[44] Hamad and co-workers[34] have fabricated periodic surface structures on a Si substrate using fs laser irradiation in acetone and further demonstrated the feasibility of Si structures grafted with Ag/Au NPs for the detection of one dye molecule (methylene blue) and two explosive molecules [2-4 dinitro toluene and 5-amino-3-nitro-l,2,4-triazole (ANTA)]. They observed superior SERS enhancements and better reproducibility from Ag/Au NP-embedded Si periodic-structured substrates because of the localization of the NPs, resulting in a higher number of hotspots along with an increased SPR strength from the Si periodic structure-embedded Ag/Au NPs.[34] All these studies have demonstrated that apart from improving the SERS performance of individual plasmonic substrates, which is a difficult proposition, another easier way is to combine two nanomaterials (either plasmonic or both plasmonic and nonplasmonic) to achieve higher enhancements in the Raman signals and thereby achieve superior limits of detection. Furthermore, a recent report by Pavlov et al. demonstrated the broad-band SERS performance of a combination of two plasmonic materials in biosensing application.[39]

The present study demonstrates such improvements in the SERS sensitivity and reproducibility by utilizing the hybrid SERS substrates (laser-processed Ag/Au embedded with Au nanostars) as compared to our earlier studies.[34,37,42] The fabrication of hybrid SERS substrates involves a two-step process in which (i) the fabrication of roughened surface structures on Ag/Au using picosecond (ps) laser ablation in air is achieved initially, followed by the (ii) synthesis of Au nanostars using the wet chemical method. Furthermore, these laser-processed Ag and Au substrates are embedded with Au nanostars and then utilized for SERS detection. The hybrid SERS substrates exploited for the trace-level detection of various analytes such as Nile blue (NB), a pesticide (thiram), and ammonium nitrate (AN). The fabricated substrates permit the detection of a 50 pM concentration of NB, a 5 nM concentration of thiram, and a 5 μM concentration of AN. The combination of ps laser-processed structures and Au nanostars provides a tangible way to achieve a greater number of hotspots in the regions of laser-processed portions along with embedded nanostars that could lead to the achievement of higher detection limits along with superior reproducibility over large areas.

EXPERIMENTAL SECTION

Methods and Materials. Chloroauric acid ($HAuCl_4\cdot 3H_2O$), sodium hydroxide (NaOH), ethanol, dimethylformamide (DMF), poly(*N*-vinyl-2-pyrrolidone) (PVP-40000 MW), and analyte molecules such as thiram ($C_6H_{12}N_2S_4$), ammonium nitrate (NH_4NO_3), and Nile blue ($C_{20}H_{20}ClN_3O$) were purchased from M/s Sigma-Aldrich. All reagents used in this study were analytically pure (99.9%), and the glassware was cleaned properly before conducting the experiments.

Synthesis of Au Nanostars. Au nanostars were synthesized using the colloidal chemical method by following a simple approach reported by Kamalesh et al.[2] In this study, polyvinyl pyrrolidone (PVP, MW ∼ 40k) was utilized as the reducing/capping agent. In brief, 10 mL of 5 mM PVP was dissolved in dimethylformamide (DMF) mixed with 1.5 mM concentration of sodium hydroxide (NaOH) and 0.27 mM concentration of $HAuCl_4\cdot 3H_2O$ and stirred continuously using a magnetic stirrer under ambient conditions. A color change in the solution was observed after 30 min and then collected in air-tight vials. Furthermore, the colloidal solution was centrifuged four times in ethanol to remove any excess PVP present. After centrifugation, the obtained nanostars were dispersed in distilled water and utilized for further studies.

Synthesis of Ag and Au NSs Using Laser Ablation. Ag and Au NSs were fabricated through ps laser ablation of the Ag/Au target in ambient air. Laser ablation experiments were implemented using a Nd: YAG laser delivering 30 ps pulses at a wavelength of 1064 nm with a repetition rate of 10 Hz. An axicon lens (base angle of 10°) was used to focus the ps laser beam normal to the Ag/Au target which was mounted on a motorized X-Y stage (Newport), and the sample was raster-scanned to avoid the ablation at a single position and to achieve roughened structures on the target surface. The ps laser ablation experiments were implemented on the bulk Ag/Au targets with a pulse energy of ∼10 mJ, and the laser-processed area was 5 mm^2 on the Ag/Au substrates. The input beam diameter was ∼10 mm, and the estimated spot size (at focus) on the target surface was ∼20 μm. A systematic study by Podagatlapalli et al. reported the focusing effect and morphological evolution of NSs by ablation on the bulk Ag substrates using an axicon lens.[45] In brief, the utilization of an axicon-employing Bessel beam offers extensive advantages over conventional Gaussian beams in terms of higher depth of focus and exotic distribution of the deposited pulse energies. In the case of laser ablation, deposition of ablating energy turns out to be a critical factor, through different beam profiles/structured beams. Absorption of incident energy due to the generated

https://doi.org/10.1021/acsomega.2c01095
ACS Omega 2022, 7, 15969−15981

plasma plume, at the critical time of ablation, significantly changes with the engagement of Bessel profile ablation. In due course of Bessel beam incidence, the central lobe intensity offers the maximum fluence along with its concentric rings. The central lobe fluence can be attributed most to the fabrication of NSs, whereas the circular distribution of energy generates the additional influence in the NSs under formation. The invariance in the intensity profile of the nondiffracting beam provides another noteworthy influence toward the precise fabrication of plasmonic NSs. Taking into account the aforementioned advantageous parameters offered by the axicon ablation (in air), interesting NSs were accomplished and further engaged as SERS-active substrates.[45]

Characterization Studies. Optical absorption measurements were carried out for Au nanostars in the wavelength range of 400−1000 nm using a UV−visible absorption spectrometer (JASCO V-670). The obtained nanostars' size and shape was investigated by pipetting 2 μL of the colloidal solution on carbon-coated copper grids and dried. Later on, transmission electron microscopy (TEM, FE-Technai G2 system operated at an accelerating voltage of 300 kV) measurements were conducted. Reflectivity measurements were conducted for plain and laser-processed Ag/Au substrates using an UV−visible−NIR spectrometer (Agilent Cary 5000) in the 200−1200 nm wavelength regime. The surface topography of laser-processed regions of Ag and Au substrates was investigated by field emission scanning electron microscopy (FESEM, Carl ZEISS) and energy-dispersive X-ray spectroscopy (EDX) measurements. The nanostar morphology was also inspected by dropwise addition of 10 μL of the colloidal solution on plain Ag/Au and laser-processed Ag/Au substrates. After drying the samples, FESEM and EDX measurements were performed. After drop-casting of the nanostars, the drying process was affected by several factors such as surface tension, contact angle, roughness, and metal composition as well.

SERS Sample Preparation and Measurements. In this study, we performed all the SERS measurements using a portable Raman spectrometer (M/s B&W Tek, USA) which had an excitation and collection fiber integrated in a single probe. The spectrometer along with a laptop weighs ∼5 kg and can be carried easily in a small suitcase. Such instruments are extremely helpful for on-field studies, and the results are obtained almost immediately. The Raman probe is designed for a working distance of 5.4 mm. We have estimated the spot size on the sample to be ∼100 μm. Analyte molecules such as thiram, AN, and NB were prepared in stock solutions with a concentration of 0.5 mM by diluting them in methanol. Furthermore, the stock solution of each analyte was successively diluted to achieve lower concentrations (from 5 mM to 50 pM). The SERS substrates were prepared by dropwise addition of 10 μL of the Au nanostar solution on the glass/silicon/Ag/Au/laser-processed Ag and Au substrates having a surface area of 5 mm^2, followed by dropwise addition of the analyte (5 μL). SERS measurements for each analyte were conducted using a portable Raman spectrometer which was equipped with a continuous laser source operating at a wavelength of 785 nm. The integration time was set to 5 s, and the accumulation number was three times for each measurement. For all the SERS measurements, an input laser power of 30 mW was employed. All recorded Raman/SERS spectra were baseline-corrected using the Origin 8.5 software on the data obtained immediately after the measurements.

RESULTS AND DISCUSSION

Figure 1 shows the absorption spectra of the prepared Au nanostars. The SPR peaks of the obtained Au nanostars were

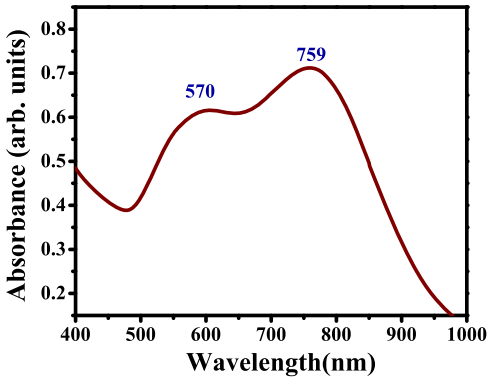

Figure 1. UV−visible absorption spectra of the synthesized Au nanostars.

observed at 570 and 759 nm. The plasmon peak noticed at 570 nm corresponds to the core of Au nanostars and the broadened peak observed at 759 nm attributed to the branches/tips of nanostars.[2] The reflectivity measurements were conducted for plain and laser-processed Ag and Au substrates, as depicted in Figure 2. Curves (i) and (ii) in Figure 2 indicate the reflectivity

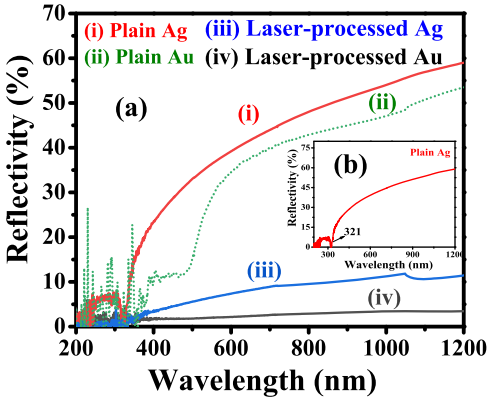

Figure 2. (a) Reflectivity of (i) plain Ag, (ii) plain Au (dotted line), (iii) laser-processed Au, and (iv) laser-processed Ag substrates, and the (b) inset shows the plain Ag reflectivity spectrum.

spectrum of plain Ag and Au substrates in which plain Ag depicted a maximum value than Au due to the higher reflectivity nature. We believe that this behavior (plain Ag/Au) is due to the fact that silver and gold were purchased locally, leaving scope for the presence of a small amount of impurities. Furthermore, the surface was not optically polished to demonstrate a sharp increase near 400 nm and close to 95% reflectivity beyond that (as is the case with optically polished silver mirrors used in the research lab). The FESEM images (data not presented here) of our surface clearly suggested the presence of roughness in our plain Ag/Au surfaces. This roughness could have reduced the reflectivity to a good extent. Due to the interband transitions in bulk Ag and Au substrates, the reflectivity fell down slowly (from 600 nm) and we observed a dip near ∼321 nm for Ag and ∼495 nm for Au.[46,47] However, in the case of the laser-processed surface of Ag [spectra (iii)] and Au [spectra (iv)], the reflectivity

https://doi.org/10.1021/acsomega.2c01095
ACS Omega 2022, 7, 15969−15981

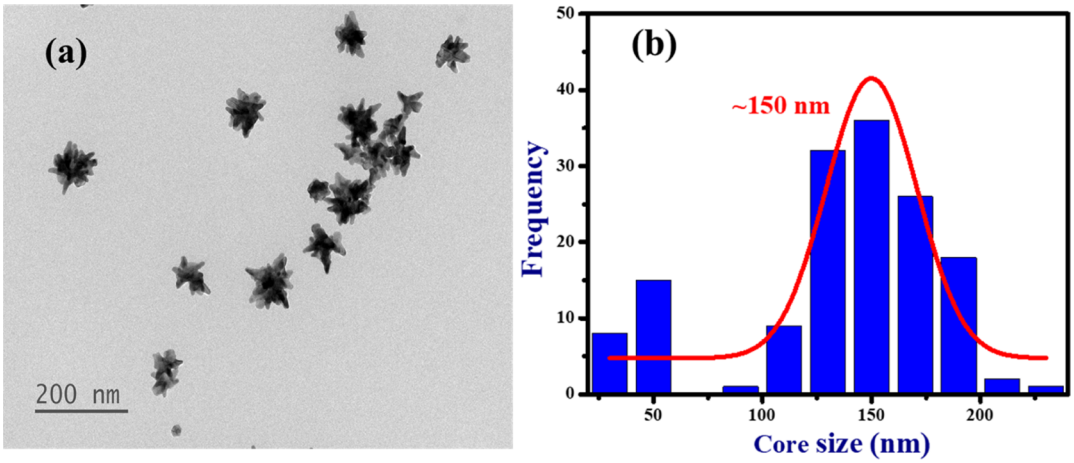

Figure 3. (a) TEM images of Au nanostars and (b) histogram plot for the core size of Au nanostars.

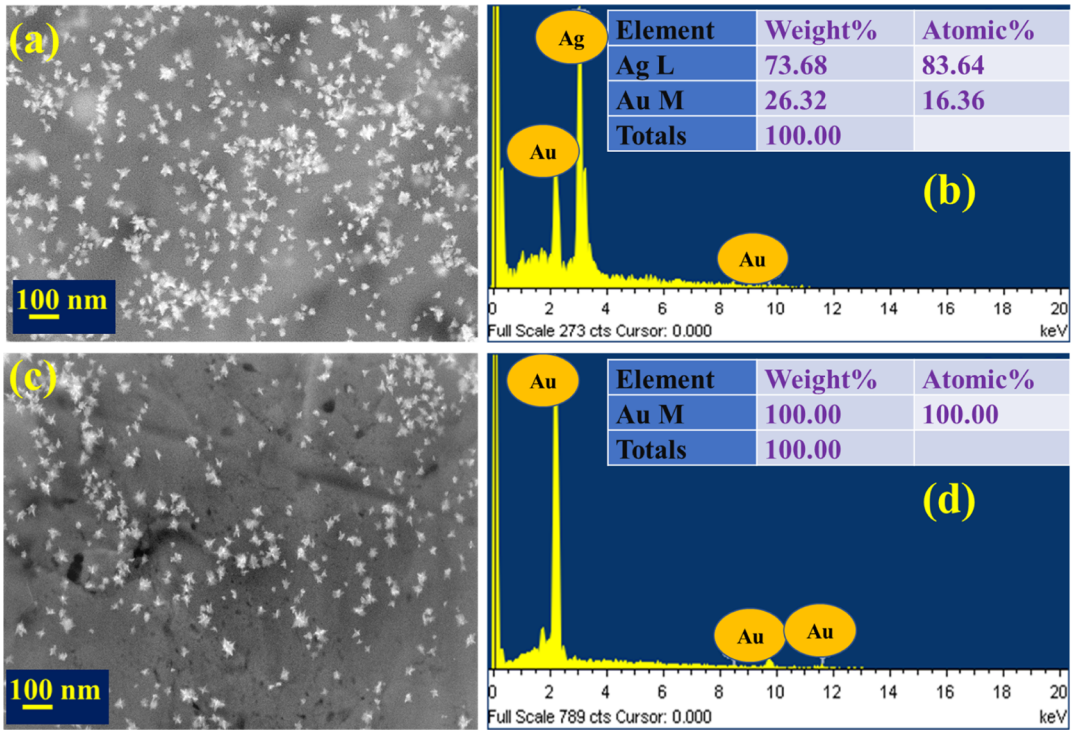

Figure 4. FESEM micrographs and the corresponding EDX spectra of Au nanostars decorated on (a,b) plain Ag and (c,d) plain Au substrates, respectively.

significantly reduced to <10%, which could be attributed to the light absorption from the nanostructured surfaces, which is well documented in the literature. Li et al.[48] demonstrated the fabrication of titanium NSs using fs laser ablation and carried out the reflectivity measurements in the range of 250−2300 nm and UV, and they found that the reflectivity was less than 2% compared to the periodic light-absorbing structures. Iyengar et al.[49] studied the optical reflection and scattering of textured titanium which was fabricated by fs laser ablation by varying laser parameters such as fluence, wavelength, incident angle, and number of pulses. They textured titanium surfaces exhibited the reflection combined with a scattering of 3% over the broad range. In our study, there could possibly be a scattering effect during the measurements, but we believe that it will be minimum in the present case.[50] However, extensive studies are imperative to confirm the role of scattering in the reduction of reflectivity.

Figure 3a depicts the TEM image of Au nanostars having more than five tips. There is a size difference in the Au nanostars and the tips, which could be ascribed to the anisotropic nucleation growth at various sites in the fabrication procedure.[2] Figure 3b shows the histogram plot for the core size of Au nanostars, which was measured using ImageJ software (S/W) by considering more than 150 nanostars, and the estimated core size was ~150 nm. Figure 4a,c depicts the FESEM micrographs of Au nanostars decorated on plain Ag and Au substrates, revealing the random distribution of nanostars throughout the substrates. Figure 4b,d illustrates the EDX spectra of the corresponding Au nanostar-decorated plain Ag and Au targets, confirming the presence of Ag and Au elements (weight percentages), as presented in the inset.

https://doi.org/10.1021/acsomega.2c01095
ACS Omega 2022, 7, 15969−15981

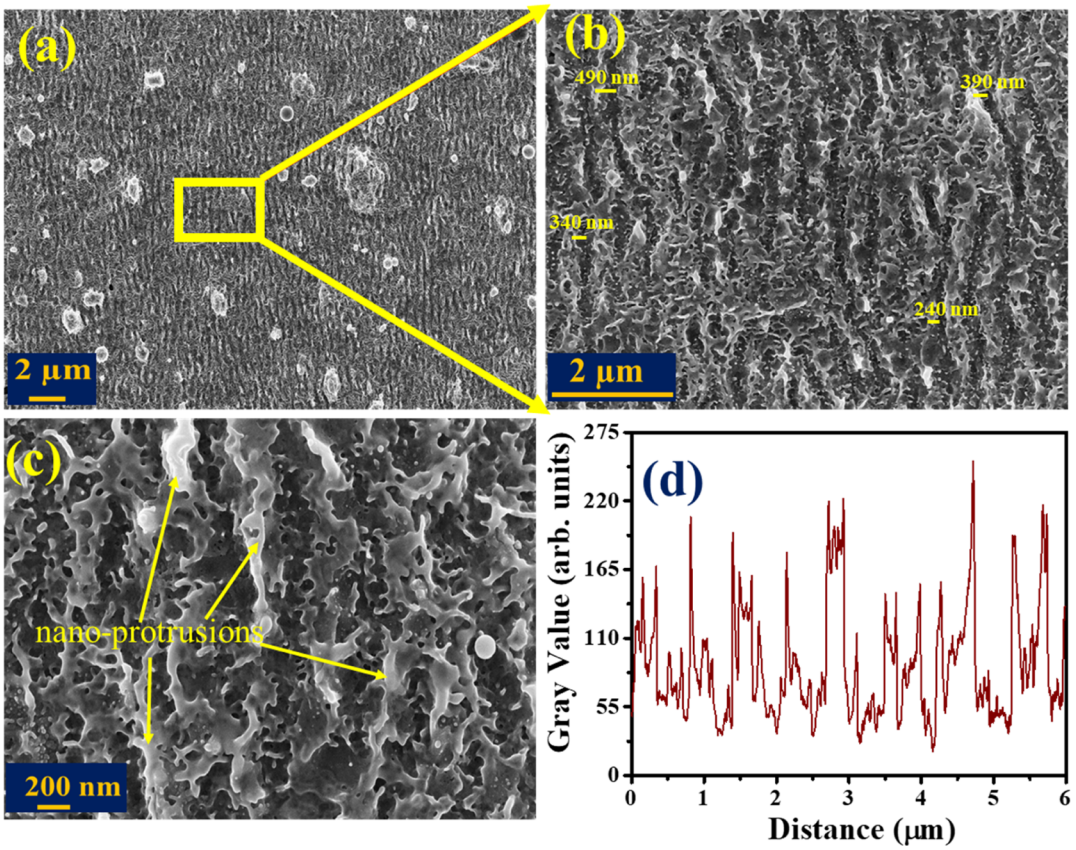

Figure 5. (a−c) FESEM micrographs of laser-processed regions of Ag obtained at different magnifications (5 KX, 20 KX, and 50 KX, respectively). Yellow square highlighted with arrow symbols in (a) is where the higher-magnification image (b) was collected. (d) Gray value (arb. units) vs horizontal position corresponding to (c) was achieved using Gwyddion S/W. Few nanoholes and nanoprotrusions are highlighted with yellow arrows in (c).

Figure 5a−c depicts the morphological features of the laser-processed portions of Ag obtained at different magnifications using the FESEM instrument. As shown in Figure 5a−c, quasi-periodic surface structures along with nanoprotrusion kind of surface features are apparent on the laser-processed regions of the Ag substrate. The quasi-periodicity varied from 240 to 490 nm (Figure 5b), estimated using Gwyddion software (S/W) and utilizing the FESEM pictures of the laser-processed Ag substrate. The accomplished periodicities on the Ag substrate were observed to be smaller than the incident laser wavelength, which can be ascribed to high-spatial-frequency laser-induced periodic surface structures (LIPSSs) or subwavelength ripples. It is already well established that two kinds of surface ripples will be observed on diverse materials when irradiated with different ultrashort laser pulses (typically few ps or fs), which are generally denoted as low-spatial frequency (LSFL) and high-spatial frequency (HSFL) LIPSSs.[27,41] The possible mechanism involved in the generation of LSFL is described based on the surface plasmon theory, where the interaction of incident laser pulses with surface plasmon polaritons occurs.[27,41] However, the origin of HSFL formation on distinct materials is still contentious and unclear, even though numerous theoretical models[51] have been proposed/documented, including self-organization,[52] molecular dynamics,[53] and thin-film theory.[54] Figure 5d illustrates the periodicity with distance accomplished by drawing the line profile on the laser-patterned area of Ag [obtained from Figure 5c using Gwyddion software (S/W)].

Figure 6a−c illustrates the FESEM pictures of laser-processed regions of Au recorded at 5 KX, 20 KX, and 50 KX magnifications, respectively. It is evident that the laser-processed regions of Au encompassed a greater number of randomly distributed nanoprotrusions fenced with nanoholes (Figure 6c). The surface profile for the laser-processed Au substrate is illustrated in Figure 6d. Furthermore, the FESEM images of the Au nanostars decorated on laser-processed regions of Ag and Au substrates are presented in Figure 7a,b, respectively. It is apparent that a higher number of nanostars were embedded in the gaps of quasi-periodic ripples and on top of the nanoprotrusions in the case of laser-processed Ag. While in case of Au, a higher number of nanostars were accommodated on top of the nanoprotrusions, and we observed that they were also occupied in gaps of nanoholes. A few nanostars are highlighted with yellow circles in Figure 7a,b for clarity.

Opting an efficient base substrate is one of the most important aspects in the SERS measurements due to the fluorescence background and/or interference of modes attained from the base substrate, which usually hinders the Raman signals of a particular analyte of interest. To investigate the effect of the base substrate in the Raman measurements, SERS data was collected for the thiram (5 μM) molecule on Au nanostar-decorated solid substrates such as (i) glass, (ii) silicon (Si), (iii) Au, and (iv) Ag substrates (shown in Figure S2). The prominent Raman modes of thiram were clearly observed from each substrate with variation in the Raman intensities. The intense Raman modes observed at 1138 and

https://doi.org/10.1021/acsomega.2c01095
ACS Omega 2022, 7, 15969−15981

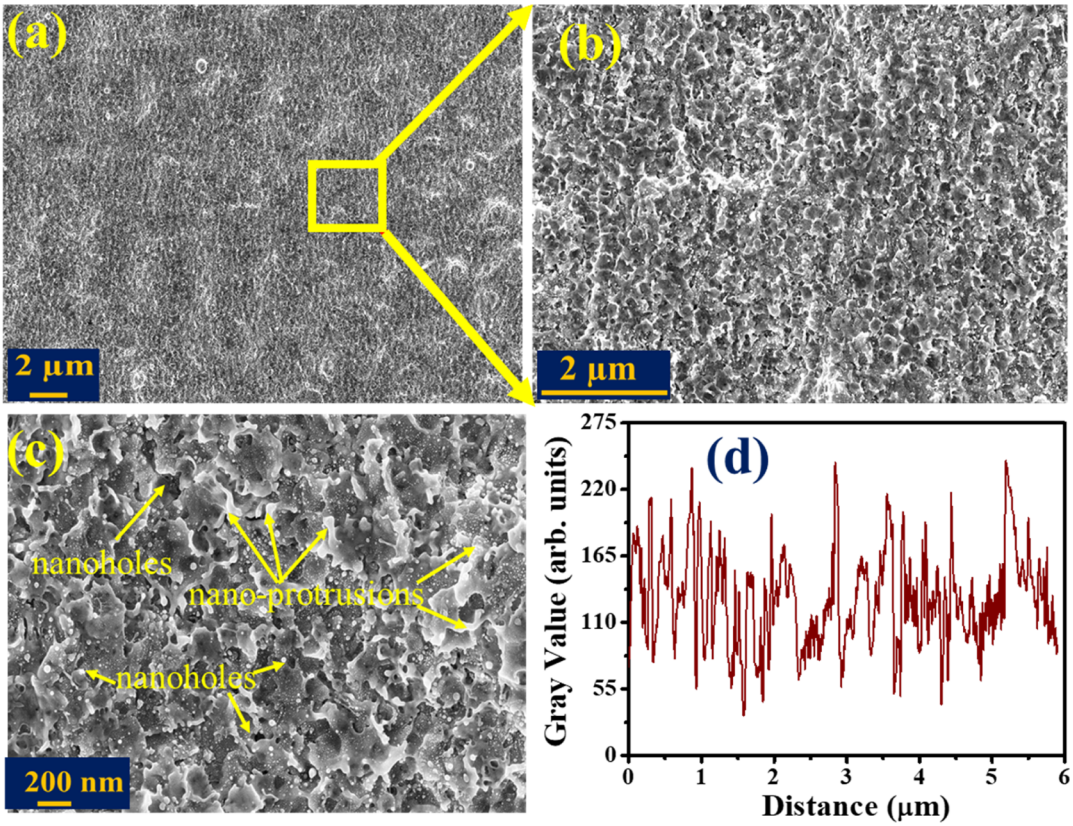

Figure 6. (a–c) FESEM micrographs of laser-processed regions of Au obtained at different magnifications (5 KX, 20 KX, and 50 KX, respectively). Yellow square highlighted with arrow symbols in (a) is where the higher-magnification image (b) was collected. (d) Gray value (arb. units) vs horizontal position corresponding to (c) achieved using Gwyddion S/W. Few nanoholes and nanoprotrusions are highlighted with yellow arrows in (c).

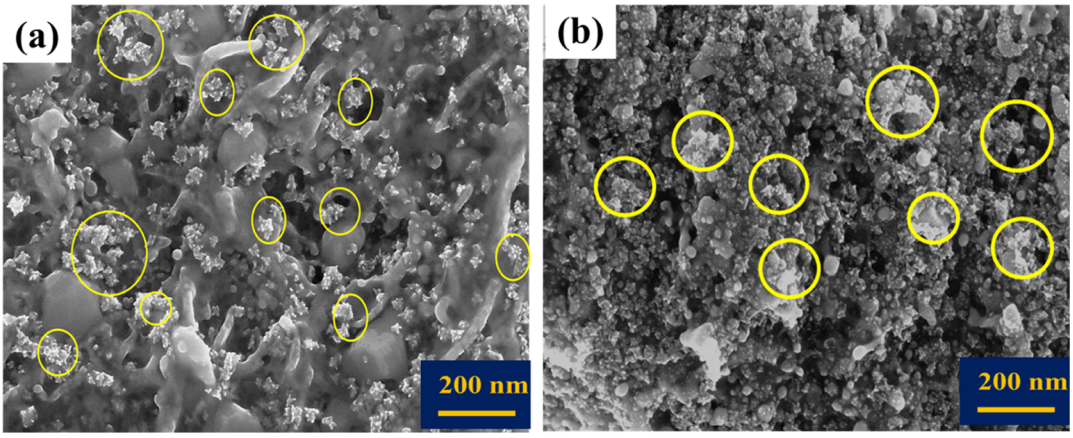

Figure 7. FESEM micrographs of Au nanostar-decorated laser-processed portions of (a) Ag and (b) Au substrates. Portions with yellow circles show a few of the highlighted nanostars.

1375 cm^{-1} were assigned to the CN stretching and symmetric deformation of CH_3, respectively. The other modes located at 560 and 940 cm^{-1} correspond to the CH bending and ring breathing, respectively, and all perceived modes well matched with earlier reported studies.[20,55] The SERS signals were observed to be higher for the Au nanostar-decorated Ag substrate among the others, and this could be attributed to the closely distributed nanostars (see the FESEM image in Figure 4a), which led to generation of a greater number of hotspots along with superior plasmonic nature of Ag, resulting in prominent SERS enhancement.

Subsequently, we continued our SERS measurements with Au nanostar-decorated plain Ag and Au substrates for the detection of various concentrations of thiram. Figure 8a illustrates the enhanced Raman signals of thiram with the concentrations ranging from 5 mM to 5 nM from the Au nanostar-decorated plain Au substrate. All prominent modes of thiram are clearly distinguishable even at the lowest concentration inspected (i.e., 5 nM). The logarithmic plot of the SERS intensity of thiram at the 1375 cm^{-1} peak with various concentrations (from 5 mM to 5 nM) established a linear relationship with a correlation coefficient (R^2) of ~0.93

https://doi.org/10.1021/acsomega.2c01095
ACS Omega 2022, 7, 15969−15981

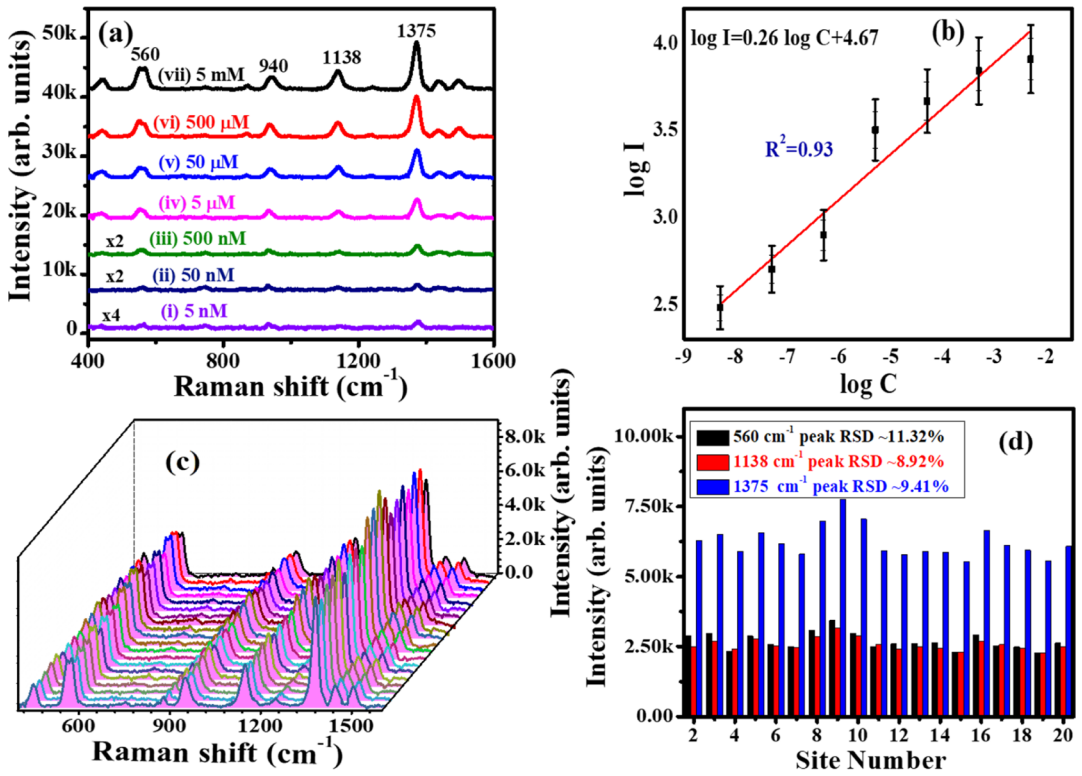

Figure 8. (a) SERS spectra of thiram obtained with the concentrations varying from 5 mM to 5 nM and collected from the Au nanostar-decorated plain Au substrate. (b) Log plot of the 1375 cm^{-1} peak SERS intensity vs thiram concentrations. (c) 3D waterfall Raman spectra plotted by collecting the data of thiram (5 mM) at 20 randomly selected sites from the Au nanostar-decorated plain Au substrate. (d) Histogram plot for the Raman intensities of 560, 1138, and 1375 cm^{-1} peaks measured at 20 sites, and the inset shows the calculated RSD values for the respective peak intensities.

(Figure 8b). The SERS substrate homogeneity was verified by collecting the thiram SERS signals at more than 20 random spots over a large area (5 mm^2) of plain Au decorated with Au nanostars, and the data is shown in Figure 8c as a 3D waterfall plot. The distribution of Au nanostars on the substrate is important for SERS enhancement.

Figure 8d depicts the estimated RSD values for the 560, 1138, and 1375 cm^{-1} Raman band intensities recorded at 20 randomly selected places, and the values were found to be ~11.32, 8.92, and 9.41%, respectively. We believe that these values can be improved further, and the improved substrates can be utilized for practical applications. The presented SERS data obtained from the Au nanostar-decorated Au substrate demonstrated the superior and satisfactory reproducibility confirming the potential of the fabricated substrate for the detection of pesticides at low concentrations. Similarly, the SERS capability of Au nanostar-decorated plain Ag was also examined with the same probe molecule (thiram).

Figure 9a depicts the concentration-dependent Raman spectra of thiram ranging from 500 μM to 5 nM obtained from the Au nanostar-decorated plain Ag substrate. It is evident that the SERS intensity of the thiram Raman bands gradually decreased with a decrease of concentration. The SERS intensity of the 1375 cm^{-1} peak with varying concentration is plotted as a logarithm plot (Figure 9b), which reveals a linear dependence of the logarithm of thiram concentration on the intensity of the prominent Raman peak (1375 cm^{-1}), and the obtained correlation coefficient (R^2) was ~0.90 (Figure 9b). Furthermore, the SERS signal consistency over the large area was yet again demonstrated by plotting the 3D waterfall and intensity histogram at 1375 cm^{-1} of thiram (5 mM) recorded from 20 randomly opted positions, and the data is shown in Figure 9c,d. The RSD values were estimated by measuring the Raman intensities at 560, 1138, and 1375 cm^{-1} modes, and the achieved values were ~16.09, 15.77, and 14.73%, respectively (the data is presented in Figure 9d).

Furthermore, a comparative study was conducted to perceive the effect of the substrate NS morphology along with decorated Au nanostars on the SERS signal enhancement. The SERS measurements conducted for the thiram molecule on laser-processed Ag and Au (without nanostars) targets along with plain surfaces (with nanostars) and laser-processed surfaces (with nanostars). The acquired SERS spectra of thiram (5 μM) on (i) and (ii) laser-processed Au/Ag, (iii) plain Au with Au nanostars, (iv) plain Ag with Au nanostars, (v) and (vi) nanostar-decorated laser-processed Au and Ag substrates are illustrated as a stack plot in Figure 10a. The calculated SERS intensities from each substrate are shown as a histogram plot, which is depicted in Figure 10b. From the presented results in Figure 10b, it is apparent that the SERS signal intensity was superior for the Au nanostar-decorated laser-processed Ag substrate among the other substrates. The estimated error bars were based on the standard deviation of the average SERS intensity at the 1375 cm^{-1} peak, obtained from repetitive SERS measurements (at least four times) (Figure 10b). The enhancement factors (EFs) were determined for each of the substrates by using the methodology reported in our earlier works[28,36,56] and were found to be 1.26×10^3, 1.83×10^3, 3.55×10^3, 4.9×10^3, 8.72×10^3, and 1.3×10^4 for laser-processed Au, laser-processed Ag, plain Au

https://doi.org/10.1021/acsomega.2c01095
ACS Omega 2022, 7, 15969−15981

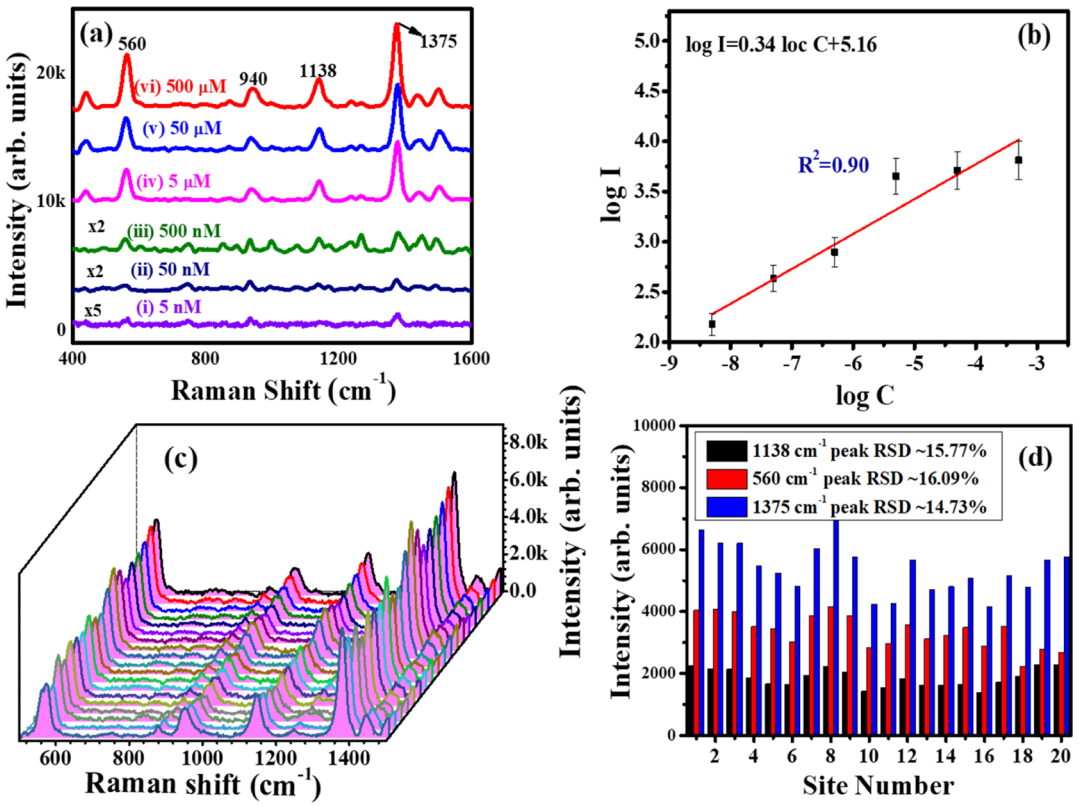

Figure 9. (a) SERS spectra of thiram obtained with concentrations varying from 500 μM to 5 nM recorded from the Au nanostar-decorated plain Ag substrate, (b) log plot of the 1375 cm^{-1} peak SERS intensity vs thiram concentration, (c) 3D waterfall Raman spectra plotted by collecting the data of thiram (5 mM) randomly at 20 sites from the Au nanostar-decorated plain Ag substrate, and (d) histogram plot for the Raman intensities of 560, 1138, and 1375 cm^{-1} peaks measured at 20 random sites, and the inset shows the calculated RSD values for the respective peak intensities.

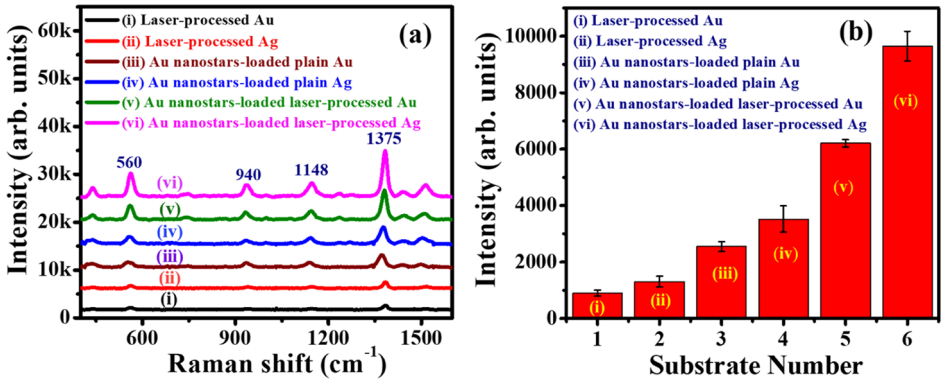

Figure 10. (a) SERS spectra of thiram (5 μM) acquired from (i) laser-processed Au (without nanostars), (ii) laser-processed Ag (without nanostars), and Au nanostars decorated on (iii) plain Au, (iv) plain Ag, (v) laser-processed Au, and (vi) laser-processed Ag substrates. (b) SERS intensity for a major mode of thiram (1375 cm^{-1}) obtained from the respective substrates. The error bars are estimated based on the standard deviation of the average SERS intensity at the 1375 cm^{-1} peak achieved by repetitive SERS measurements for four times.

(with Au nanostars), plain Ag (with Au nanostars), laser-processed Au (with Au nanostars), and laser-processed Ag substrates (with Au nanostars), respectively. Details of the EF calculations are presented in the Supporting Information. To summarize the improvements observed in the present SERS studies, nanostar-loaded ps laser-processed Ag/Au substrates showed ~3 times higher signal enhancement than plain Ag/Au substrates decorated with Au nanostars and ~8 times higher signal enhancement than only ps laser-processed Ag/Au substrates.

Kalachyova et al. have recently demonstrated the ultrasensitive detection of R6G (10^{-11} M) using multibranched Au NPs grafted on the Ag grating structure as a SERS substrate.[57] They have proposed that the achieved superior detection limit could be attributed to the plasmonic coupling and interplay between the surface plasmon polaritons of Ag grating and localized surface plasmons of Au NPs. In the present case, the Ag structure has quasi-periodic surface features surrounded with few nanoholes, which can possibly graft a greater number of nanostars, leading to the possible formation of a large number of hotspots and thereby resulting in prominent SERS enhancements. Additionally, there could be a slight variation in the surface roughness after deposition of the nanostars on the laser-processed regions of Ag, which could also contribute the

https://doi.org/10.1021/acsomega.2c01095
ACS Omega 2022, 7, 15969−15981

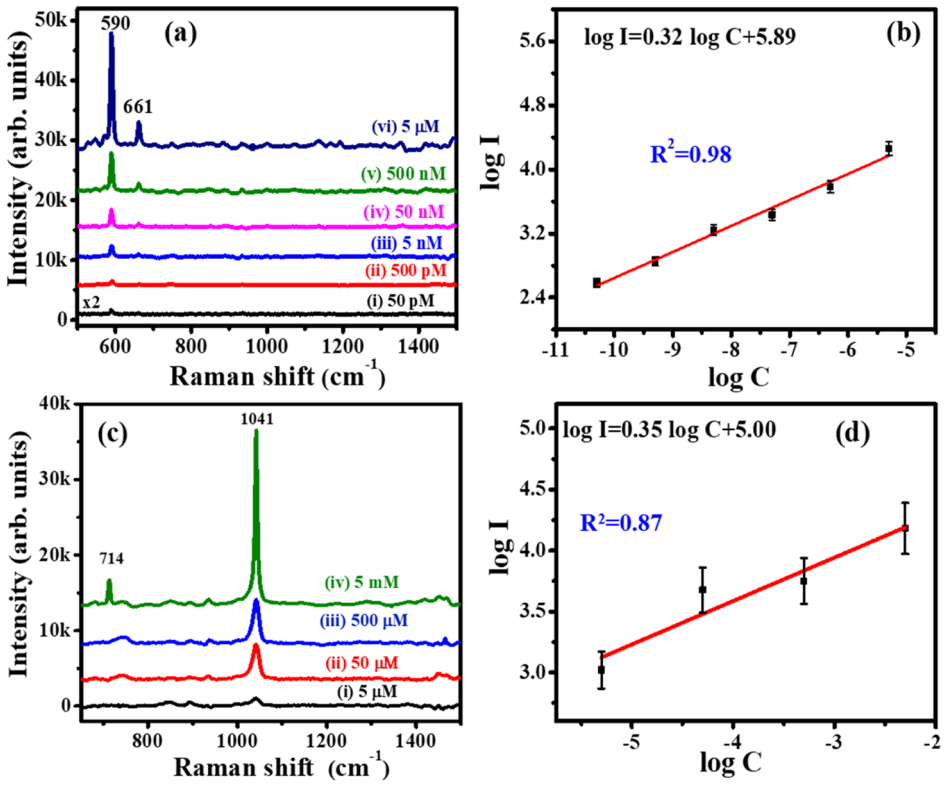

Figure 11. (a) SERS spectra of NB with the concentrations ranging from 5 μM to 50 pM recorded from the Au nanostar-decorated laser-processed Ag substrate, (b) log plot of the 590 cm^{-1} peak SERS intensity vs NB concentration, (c) SERS spectra of AN with the concentrations varying from 5 mM to 5 μM recorded from the Au nanostar-decorated laser-processed Ag substrate, and (d) log plot of the 1041 cm^{-1} peak SERS intensity vs AN concentration.

SERS enhancement further. We have estimated the surface roughness (using ImageJ software from the FESEM pictures) of laser-processed Ag and Au substrates, as well as Au nanostar-decorated laser-processed Ag and Au substrates, and the data is presented in Figure S1 of the Supporting Information. We have observed a higher surface roughness (~129 nm) for Au nanostar-decorated laser-processed Ag among the other substrates. Lee et al. have experimentally demonstrated the role of silver (Ag) film thickness and substrate roughness of polydimethylsiloxane (PDMS)/glass in the enhancement of the SERS signals.[58] Similarly, they found prominent enhancements for the silver-coated PDMS substrate compared to the glass substrate due to the thickness, as well as the roughness of PDMS. Furthermore, they have explained that the thickness of the Ag film played a significant role in the observed SERS enhancements compared to the substrate roughness. In this study, we have not performed any SERS measurements by varying the surface roughness of the substrate, but we have observed surface roughness variation before and after the deposition of nanostars on the laser-processed substrates. There is also a possibility of increasing the surface roughness by simply drop-casting a higher number of nanostars on the laser-processed substrates and plain substrates, which will most probably influence the SERS performance. In addition, the nanostar density could also affect the SERS performance and can be achieved by performing the drop-casting procedure multiple times on the same area of the base substrate. However, in our case, we have drop-cast only 10 μL of the nanostar solution on each substrate, and we believe that the density may not be the same in all cases due to diverse morphologies, surface tensions, and so forth. By drop-casting additional quantities, we can possibly make it more uniform in each case, and thereby, we can achieve better Raman signals. Wei et al. studied the influence of NS density on SERS signal enhancement.[59] They found that the SERS enhancements increased with increasing density up to a certain level and then reduced. To get a better understanding on the effect of surface roughness/nanostar density, more detailed investigations are needed and will be considered in future. In addition, the concentration-dependent SERS spectra and linear plot are presented in the Supporting Information (Figure S3a,b). The signal reproducibility spectra of thiram and variation of SERS intensity for major bands at different positions obtained from the Au nanostar-decorated laser-processed Ag substrate are shown in Figure S3c,d. The estimated RSD values were found to be 7.96, 5.43, and 5.13% for the prominent Raman mode intensities of 560, 1138 and 1375 cm^{-1}, respectively (Figure S3d).

Due to the higher SERS sensitivity and better signal reproducibility, the Au nanostar-loaded laser-processed Ag substrate was opted further for the detection of other analytes such as NB and AN. The SERS spectra of NB at different concentrations ranging from 5 μM to 50 pM recorded from the Au nanostar-decorated laser-processed Ag substrate are illustrated in Figure 11a. The NB Raman bands were located at 590 and 661 cm^{-1} and are associated with the C−C−C and C−N−C deformations and in-plane C−C−C deformation.[43] The NB major peak intensities were significantly enhanced while increasing the concentration, and the detected lower concentration was ~5 × 10^{-11} M. Even at the 50 pM concentration, major Raman modes of NB were clearly distinguishable, revealing the higher sensitivity of the Au

https://doi.org/10.1021/acsomega.2c01095
ACS Omega 2022, 7, 15969−15981

nanostar-loaded laser-processed Ag substrate. A logarithmic plot between the SERS signal intensity for the prominent mode of NB located at 590 cm^{-1} with varying concentration is shown in Figure 11b. The correlation coefficient (R^2) was found to be 0.98, illustrating the detection sensitivity of the Au nanostar-decorated patterned Ag substrate. SERS signal reproducibility was also evaluated for the Au nanostar-loaded laser-processed Ag target by collecting the Raman data of NB (5 μM) at 25 randomly chosen spots, and the data was plotted as 3D waterfall spectra, as shown in Figure S4a. The measured RSD values were 13.84 and 14.14% for the Raman peaks at 590 and 661 cm^{-1}, respectively (the data is shown in Figure S4b). The spot size of our portable Raman spectrometer is typically 100 μm (unlike in the micro-Raman systems whose typical spot sizes are 1−2 μm), and the signal we collected was from such a large area. We have demonstrated the reproducibility of the SERS/Raman data by performing measurements at randomly selected 20−25 locations over a large area of the substrate, which was ∼5 mm^2. These measurements demonstrate that such an exercise can be carried out by a novice also in the field.

The efficacy of the Au nanostar-loaded laser-processed Ag SERS substrate was again tested by detecting the AN. The enhanced Raman intensities for various concentrations of AN (from 5 mM to 5 μM) observed from the Au nanostar-decorated laser-processed Ag substrate are illustrated in Figure 11c. The strongest Raman band of AN appeared at 1041 cm^{-1} and is associated with the NO_3^- symmetric stretch, and the observed peaks matched well with the earlier literature.[56,60] The detected concentration of AN (5 μM) was moderate among the other molecules, which could be ascribed to the utilized polymer (PVP) in the synthesis that might have passivated the surface of Au nanostars and decreased the interaction between AN and nanostars, resulting in lower SERS enhancement. The SERS sensitivity of Au nanostars for explosive molecules can be further improved by reducing the thickness of the PVP layer (shell) or completely eliminating it, which needs additional and detailed investigations.[2]

Detailed calculations of the EFs are provided in the Supporting Information (Table S1), and the EFs obtained for the Au nanostar-decorated laser-processed Ag substrates were 0.5 × 10^6, 1.98 × 10^6, and 0.2 × 10^4 for thiram, NB, and AN, respectively. The normal Raman spectra of each analyte were recorded using a plain Ag substrate, and the data is provided in Figure S5 of the Supporting Information. Figure 11d depicts a linear plot between the AN SERS signal intensity at 1041 cm^{-1} peak versus the concentration, and the obtained correlation coefficient (R^2) was ∼0.87. Furthermore, the detected concentration levels were different for different analyte molecules, which mainly depend on numerous factors such as (a) binding affinity of a specific analyte molecule with the SERS substrate and also the disparity in their Raman cross-sections at a particular excitation wavelength,[61−64] (b) distance between the nanostars and the analyte molecule,[65] (c) number of produced hotspots,[65] (d) number of molecules under the laser-probed area,[65] and (e) orientation of the analyte molecule with respect to the NSs.[62,65] Additionally, the details of SERS detection limits and estimated EFs for thiram, NB, and AN of a few earlier reported studies are compared with our substrates (obtained in this study), and the results are summarized in Table S2 of the supporting information.

Ag as a plasmonic metal has superior electric near-field enhancements and, consequently, better SERS performance than Au but suffers from oxidation, and the difference for Ag/Au substrates observed in this study is in line with what is expected from the literature.[66] Although these substrates can detect diverse analyte molecules, it is imperative to optimize them for detecting the molecules of interest. There are several avenues for the improvement of these substrates. For example, drop-casting a greater number of nanostars will increase the hotspots. Our future studies will also focus on (a) optimizing the nanostars with a higher number and sharper tips and (b) improving the SERS performance of laser-processed Ag and Au substrates.

CONCLUSIONS

In summary, we have successfully achieved hybrid SERS platforms by embedding chemically prepared Au nanostars on ps laser-processed plasmonic targets (Ag and Au). These hybrid SERS substrates were efficiently utilized in the detection of diverse analyte molecules such as thiram, NB, and AN at miniscule concentrations of 5 nM, 50 pM, and 5 μM, respectively. Additionally, comparative SERS studies were performed in detail for Au nanostar-embedded (a) non-plasmonic, (b) plasmonic, and (c) laser-processed plasmonic substrates. The obtained SERS data demonstrated that the Au nanostar-loaded laser-processed Ag substrates exhibited better enhancements with an improved sensitivity and reproducibility for the detection of all analytes investigated in the present study. The possible explanation for this observation could be that the nanostructured surface had plenty of sharp tips and edges that promoted the lightning rod effect along with quasi-periodic NSs. The achieved EFs from the Au nanostar-decorated laser-processed Ag substrate were 0.5 × 10^6, 1.98 × 10^6, and 0.2 × 10^4 for thiram, NB, and AN, respectively, with a reasonable reproducibility (RSD < 20%) for three different analytes. Finally, we believe that mixing different plasmon-active materials can be used to achieve broadband enhancements at various SERS pump wavelengths.[39]

ASSOCIATED CONTENT

Supporting Information

The Supporting Information is available free of charge at https://pubs.acs.org/doi/10.1021/acsomega.2c01095.

Surface roughness variation of different substrates investigated; SERS spectra of thiram (5 μM) on different plain substrates such as glass, Si, Au, and Ag decorated with Au nanostars; thiram SERS spectra at different concentrations, log plot of SERS intensity versus concentration, waterfall/histogram plots of the reproducibility spectra; NB reproducible SERS spectra (waterfall/histogram plots); normal Raman spectra of thiram, NB, and AN recorded from the plain Ag substrate; EF calculations for thiram, NB, and AN from the Au nanostar-decorated laser-processed Ag substrate; and comparison of SERS detection limits and estimated EFs for thiram, AN, and NB with the present study (PDF)

AUTHOR INFORMATION

Corresponding Author

Venugopal Rao Soma − *Advanced Centre of Research in High Energy Materials (**ACRHEM**), University of Hyderabad, Hyderabad 500046 Telangana, India;* orcid.org/0000-0001-5361-7256; Email: soma_venu@uohyd.ac.in

https://doi.org/10.1021/acsomega.2c01095
ACS Omega 2022, 7, 15969−15981

Authors

Jagannath Rathod − *Advanced Centre of Research in High Energy Materials (**ACRHEM**), University of Hyderabad, Hyderabad 500046 Telangana, India*

Chandu Byram − *Advanced Centre of Research in High Energy Materials (**ACRHEM**), University of Hyderabad, Hyderabad 500046 Telangana, India*

Ravi Kumar Kanaka − *School of Physics, University of Hyderabad, Hyderabad 500046 Telangana, India*

Moram Sree Satya Bharati − *Advanced Centre of Research in High Energy Materials (**ACRHEM**), University of Hyderabad, Hyderabad 500046 Telangana, India*

Dipanjan Banerjee − *Advanced Centre of Research in High Energy Materials (**ACRHEM**), University of Hyderabad, Hyderabad 500046 Telangana, India*

Mangababu Akkanaboina − *School of Physics, University of Hyderabad, Hyderabad 500046 Telangana, India*

Complete contact information is available at: https://pubs.acs.org/10.1021/acsomega.2c01095

Notes

The authors declare no competing financial interest.

■ ACKNOWLEDGMENTS

V.R.S. acknowledges the DRDO [ERIP/ER/1501138/M/01/319/D(R&D)] for financial support through ARCHEM, University of Hyderabad (UoH). V.R.S. also thanks the UoH for support through a project under the aegis of the Institute of Eminence (# UOH/IOE/RC1/RC1-20-016). The IoE grant was received from the MHRD, India [notification F11/9/2019-U3(A)]. D.B. thanks the PRMF from the Government of India for funding. The authors thank the Director, ACRHEM (Dr. V. Kameswara Rao) for his support and encouragement.

■ REFERENCES

(1) Li, J.; Lin, H.; Zhang, X.; Li, M. Seed shape-controlled, facet-selective growth of superspiky gold nanocrystals for biosensing applications. *J. Mater. Chem. C* **2021**, *9*, 8694−8704.

(2) Nehra, K.; Pandian, S. K.; Byram, C.; Moram, S. S. B.; Soma, V. R. Quantitative analysis of catalysis and SERS performance in hollow and star-shaped Au nanostructures. *J. Phys. Chem. C* **2019**, *123*, 16210−16222.

(3) Turino, M.; Pazos-Perez, N.; Guerrini, L.; Alvarez-Puebla, R. A. Positively-charged plasmonic nanostructures for SERS sensing applications. *RSC Adv.* **2022**, *12*, 845−859.

(4) Mobed, A.; Hasanzadeh, M.; Seidi, F. Anti-bacterial activity of gold nanocomposites as a new nanomaterial weapon to combat photogenic agents: recent advances and challenges. *RSC Adv.* **2021**, *11*, 34688−34698.

(5) Nehra, K.; Pandian, S. K.; Bharati, M. S. S.; Soma, V. R. Enhanced catalytic and SERS performance of shape/size controlled anisotropic gold nanostructures. *New J. Chem.* **2019**, *43*, 3835−3847.

(6) Ortiz-Castillo, J. E.; Gallo-Villanueva, R. C.; Madou, M. J.; Perez-Gonzalez, V. H. Anisotropic gold nanoparticles: A survey of recent synthetic methodologies. *Coord. Chem. Rev.* **2020**, *425*, 213489.

(7) Pazos-Perez, N.; Guerrini, L.; Alvarez-Puebla, R. A. Plasmon tunability of gold nanostars at the tip apexes. *ACS Omega* **2018**, *3*, 17173−17179.

(8) Oliveira, M. J.; Cunha, I.; de Almeida, M. P.; Calmeiro, T.; Fortunato, E.; Martins, R.; Pereira, L.; Byrne, H. J.; Pereira, E.; Águas, H.; et al. Reusable and highly sensitive SERS immunoassay utilizing gold nanostars and a cellulose hydrogel-based platform. *J. Mater. Chem. B* **2021**, *9*, 7516−7529.

(9) Khlebtsov, B.; Panfilova, E.; Khanadeev, V.; Khlebtsov, N. Improved size-tunable synthesis and SERS properties of Au nanostars. *J. Nanopart. Res.* **2014**, *16*, 1−12.

(10) Jimenez de Aberasturi, D.; Serrano-Montes, A. B.; Langer, J.; Henriksen-Lacey, M.; Parak, W. J.; Liz-Marzán, L. M. Surface enhanced Raman scattering encoded gold nanostars for multiplexed cell discrimination. *Chem. Mater.* **2016**, *28*, 6779−6790.

(11) López-Lorente, Á. I. Recent developments on gold nanostructures for surface enhanced Raman spectroscopy: particle shape, substrates and analytical applications. A review. *Anal. Chim. Acta* **2021**, *1168*, 338474.

(12) Bharati, M. S. S.; Soma, V. R.; Soma, V. R. Flexible SERS substrates for hazardous materials detection: recent advances. *Opto-Electron. Adv.* **2021**, *4*, 210048.

(13) Zhang, Q.; Large, N.; Wang, H. Gold nanoparticles with tipped surface structures as substrates for single-particle surface-enhanced Raman spectroscopy: concave nanocubes, nanotrisoctahedra, and nanostars. *ACS Appl. Mater. Interfaces* **2014**, *6*, 17255−17267.

(14) Lu, G.; Johns, A. J.; Neupane, B.; Phan, H. T.; Cwiertny, D. M.; Forbes, T. Z.; Haes, A. J. Matrix-independent surface-enhanced Raman scattering detection of uranyl using electrospun amidoximated polyacrylonitrile mats and gold nanostars. *Anal. Chem.* **2018**, *90*, 6766−6772.

(15) Kartashova, A. D.; Gonchar, K. A.; Chermoshentsev, D. A.; Alekseeva, E. A.; Gongalsky, M. B.; Bozhev, I. V.; Eliseev, A. A.; Dyakov, S. A.; Samsonova, J. V.; Osminkina, L. A. Surface-Enhanced Raman Scattering-Active Gold-Decorated Silicon Nanowire Substrates for Label-Free Detection of Bilirubin. *ACS Biomater. Sci. Eng.* **2021**, DOI: 10.1021/acsbiomaterials.1c00728.

(16) Zhang, C.; Chen, S.; Jiang, Z.; Shi, Z.; Wang, J.; Du, L. Highly Sensitive and Reproducible SERS Substrates Based on Ordered Micropyramid Array and Silver Nanoparticles. *ACS Appl. Mater. Interfaces* **2021**, *13*, 29222.

(17) Cao, W.; Jiang, L.; Hu, J.; Wang, A.; Li, X.; Lu, Y. Optical field enhancement in Au nanoparticle-decorated nanorod arrays prepared by femtosecond laser and their tunable surface-enhanced Raman scattering applications. *ACS Appl. Mater. Interfaces* **2018**, *10*, 1297−1305.

(18) Bär, J.; de Barros, A.; de Camargo, D. H. S.; Pereira, M. P.; Merces, L.; Shimizu, F. M.; Sigoli, F. A.; Bufon, C. C. B.; Mazali, I. O. Silicon microchannel-driven Raman scattering enhancement to improve gold nanorod functions as a SERS substrate toward single-molecule detection. *ACS Appl. Mater. Interfaces* **2021**, *13*, 36482−36491.

(19) Ko, H.; Singamaneni, S.; Tsukruk, V. V. Nanostructured surfaces and assemblies as SERS media. *Small* **2008**, *4*, 1576−1599.

(20) Naqvi, T. K.; Bajpai, A.; Bharati, M. S. S.; Kulkarni, M. M.; Siddiqui, A. M.; Soma, V. R.; Dwivedi, P. K. Ultra-sensitive Reusable SERS Sensor for Multiple Hazardous Materials Detection on Single Platform. *J. Hazard. Mater.* **2020**, *407*, No. 124353.

(21) Shukla, P.; Waugh, D. G.; Lawrence, J.; Vilar, R. Laser surface structuring of ceramics, metals and polymers for biomedical applications: A review. *Laser Surface Modification of Biomaterials*; Woodhead Publishing, 2016; pp 281−299.

(22) Naqvi, T. K.; Sree Satya Bharati, M.; Srivastava, A. K.; Kulkarni, M. M.; Siddiqui, A. M.; Rao, S. V.; Dwivedi, P. K. Hierarchical laser-patterned silver/graphene oxide hybrid SERS sensor for explosive detection. *ACS Omega* **2019**, *4*, 17691−17701.

(23) Sun, X.; Li, H. A review: nanofabrication of surface-enhanced Raman spectroscopy (SERS) substrates. *Curr. Nanosci.* **2016**, *12*, 175−183.

(24) Raillard, B.; Mücklich, F. Ablation effects of femtosecond laser functionalization on surfaces. In *Laser Surface Engineering*, Elsevier, 2015; pp 565-581. DOI: 10.1016/b978-1-78242-074-3.00024-6

(25) Li, L.; Hong, M.; Schmidt, M.; Zhong, M.; Malshe, A.; Huis in'tVeld, B.; Kovalenko, V. Laser nano-manufacturing−state of the art and challenges. *CIRP Ann.* **2011**, *60*, 735−755.

(26) Sugioka, K.; Cheng, Y. Ultrafast lasers—reliable tools for advanced materials processing. *Light: Sci. Appl.* **2014**, *3*, No. e149.

(27) Vorobyev, A. Y.; Guo, C. Direct femtosecond laser surface nano/microstructuring and its applications. *Laser Photonics Rev.* **2013**, *7*, 385−407.
(28) Byram, C.; Moram, S. S. B.; Soma, V. R. SERS based detection of multiple analytes from dye/explosive mixtures using picosecond laser fabricated gold nanoparticles and nanostructures. *Analyst* **2019**, *144*, 2327−2336.
(29) Rao, S. V.; Podagatlapalli, G. K.; Hamad, S. Ultrafast laser ablation in liquids for nanomaterials and applications. *J. Nanosci. Nanotechnol.* **2014**, *14*, 1364−1388.
(30) Hamad, S.; Podagatlapalli, G. K.; Mohiddon, M. A.; Soma, V. R. Cost effective nanostructured copper substrates prepared with ultrafast laser pulses for explosives detection using surface enhanced Raman scattering. *Appl. Phys. Lett.* **2014**, *104*, 263104.
(31) Hamad, S.; Podagatlapalli, G. K.; Tewari, S. P.; Rao, S. V. Influence of picosecond multiple/single line ablation on copper nanoparticles fabricated for surface enhanced Raman spectroscopy and photonics applications. *J. Phys. D: Appl. Phys.* **2013**, *46*, 485501.
(32) Marrapu, H.; Avasarala, R.; Soma, V. R.; Balivada, S. K.; Podagatlapalli, G. K. Silver nanoribbons achieved by picosecond ablation using cylindrical focusing and SERS-based trace detection of TNT. *RSC Adv.* **2020**, *10*, 41217−41228.
(33) Sree Satya Bharati, M.; Byram, C.; Soma, V. R. Femtosecond Laser Fabricated Ag@Au and Cu@Au Alloy Nanoparticles for Surface Enhanced Raman Spectroscopy Based Trace Explosives Detection. *Front. Phys.* **2018**, *6*, 28.
(34) Hamad, S.; Bharati Moram, S. S.; Yendeti, B.; Podagatlapalli, G. K.; Nageswara Rao, S. V. S.; Pathak, A. P.; Mohiddon, M. A.; Soma, V. R. Femtosecond laser-induced, nanoparticle-embedded periodic surface structures on crystalline silicon for reproducible and multi-utility SERS platforms. *ACS Omega* **2018**, *3*, 18420−18432.
(35) Mangababu, A.; Sai Prasad Goud, R.; Byram, C.; Rathod, J.; Banerjee, D.; Rao Soma, V.; Nageswara Rao, S. V. S. Multi-functional gallium arsenide nanoparticles and nanostructures fabricated using picosecond laser ablation. *Appl. Surf. Sci.* **2022**, *589*, 152802.
(36) Byram, C.; Soma, V. R. 2, 4-dinitrotoluene detected using portable Raman spectrometer and femtosecond laser fabricated Au−Ag nanoparticles and nanostructures. *Nano-Struct. Nano-Objects* **2017**, *12*, 121−129.
(37) Moram, S. S. B.; Shaik, A. K.; Byram, C.; Hamad, S.; Soma, V. R. Instantaneous trace detection of nitro-explosives and mixtures with nanotextured silicon decorated with Ag−Au alloy nanoparticles using the SERS technique. *Anal. Chim. Acta* **2020**, *1101*, 157−168.
(38) Kuchmizhak, A.; Pustovalov, E.; Syubaev, S.; Vitrik, O.; Kulchin, Y.; Porfirev, A.; Khonina, S.; Kudryashov, S.; Danilov, P.; Ionin, A. On-fly femtosecond-laser fabrication of self-organized plasmonic nanotextures for chemo-and biosensing applications. *ACS Appl. Mater. Interfaces* **2016**, *8*, 24946−24955.
(39) Pavlov, D.; Syubaev, S.; Cherepakhin, A.; Sergeev, A.; Vitrik, O.; Zakharenko, A.; Danilov, P.; Saraeva, I.; Kudryashov, S.; Porfirev, A.; Kuchmizhak, A. Ultrafast laser printing of self-organized bimetallic nanotextures for multi-wavelength biosensing. *Sci. Rep.* **2018**, *8*, 16489−10.
(40) Bérubé, V.; Radtke, G.; Dresselhaus, M.; Chen, G. Size effects on the hydrogen storage properties of nanostructured metal hydrides: A review. *Int. J. Energy Res.* **2007**, *31*, 637−663.
(41) Bonse, J.; Höhm, S.; Kirner, S. V.; Rosenfeld, A.; Krüger, J. Laser-induced periodic surface structures—A scientific evergreen. *IEEE J. Sel. Top. Quantum Electron.* **2016**, *23*, 9000615.
(42) Byram, C.; Moram, S. S. B.; Soma, V. R. Surface-enhanced Raman scattering studies of gold-coated ripple-like nanostructures on iron substrate achieved by femtosecond laser irradiation in water. *J. Raman Spectrosc.* **2019**, *50*, 1103−1113.
(43) Chandu, B.; Sree Satya Bharati, M.; Albrycht, P.; Rao, S. V. Fabrication of nanocages on nickel using femtosecond laser ablation and trace level detection of malachite green and Nile blue dyes using surface enhanced Raman spectroscopic technique. *Opt. Laser Technol.* **2020**, *131*, 106454.
(44) Moram, S. S. B.; Byram, C.; Soma, V. R. Gold-nanoparticle-and nanostar-loaded paper-based SERS substrates for sensing nanogram-level Picric acid with a portable Raman spectrometer. *Bull. Mater. Sci.* **2020**, *43*, 53.
(45) Podagatlapalli, G. K.; Hamad, S.; Mohiddon, M. A.; Rao, S. V. Fabrication of nanoparticles and nanostructures using ultrafast laser ablation of silver with Bessel beams. *Laser Phys. Lett.* **2015**, *12*, 036003.
(46) Krishna Podagatlapalli, G.; Hamad, S.; Tewari, S. P.; Sreedhar, S.; Prasad, M. D.; Venugopal Rao, S. Silver nano-entities through ultrafast double ablation in aqueous media for surface enhanced Raman scattering and photonics applications. *J. Appl. Phys.* **2013**, *113*, 073106.
(47) Osorio, M. F.; Salazar, A.; Prieto, F.; Boulanger, P.; Figueroa, P. Three-dimensional digitization of highly reflective and transparent objects using multi-wavelength range sensing. *Mach. Vis. Appl.* **2012**, *23*, 761−772.
(48) Li, X.; Li, M.; Liu, H. Effective strategy to achieve a metal surface with ultralow reflectivity by femtosecond laser fabrication. *Chin. Opt. Lett.* **2021**, *19*, 051401.
(49) Iyengar, V. V.; Nayak, B. K.; Gupta, M. C. Ultralow reflectance metal surfaces by ultrafast laser texturing. *Appl. Opt.* **2010**, *49*, 5983−5988.
(50) Schade, H.; Smith, Z. E. Mie scattering and rough surfaces. *Appl. Opt.* **1985**, *24*, 3221−3226.
(51) Bonse, J.; Gräf, S. Maxwell Meets Marangoni—A Review of Theories on Laser-Induced Periodic Surface Structures. *Laser Photonics Rev.* **2020**, *14*, 2000215.
(52) Varlamova, O.; Bounhalli, M.; Reif, J. Influence of irradiation dose on laser-induced surface nanostructures on silicon. *Appl. Surf. Sci.* **2013**, *278*, 62−66.
(53) Shugaev, M. V.; Gnilitskyi, I.; Bulgakova, N. M.; Zhigilei, L. V. Mechanism of single-pulse ablative generation of laser-induced periodic surface structures. *Phys. Rev. B* **2017**, *96*, 205429.
(54) Miyaji, G.; Miyazaki, K. Origin of periodicity in nanostructuring on thin film surfaces ablated with femtosecond laser pulses. *Opt. Express* **2008**, *16*, 16265−16271.
(55) Picone, A. L.; Rizzato, M. L.; Lusi, A. R.; Romano, R. M. Stamplike flexible SERS substrate for in-situ rapid detection of thiram residues in fruits and vegetables. *Food Chem.* **2022**, *373*, 131570.
(56) Satya Bharati, M. S.; Chandu, B.; Rao, S. V. Explosives sensing using Ag−Cu alloy nanoparticles synthesized by femtosecond laser ablation and irradiation. *RSC Adv.* **2019**, *9*, 1517−1525.
(57) Kalachyova, Y.; Mares, D.; Jerabek, V.; Ulbrich, P.; Lapcak, L.; Svorcik, V.; Lyutakov, O. Ultrasensitive and reproducible SERS platform of coupled Ag grating with multibranched Au nanoparticles. *Phys. Chem. Chem. Phys.* **2017**, *19*, 14761−14769.
(58) Lee, C.; Robertson, C. S.; Nguyen, A. H.; Kahraman, M.; Wachsmann-Hogiu, S. Thickness of a metallic film, in addition to its roughness, plays a significant role in SERS activity. *Sci. Rep.* **2015**, *5*, 11644.
(59) Wei, S.; Zheng, M.; Xiang, Q.; Hu, H.; Duan, H. Optimization of the particle density to maximize the SERS enhancement factor of periodic plasmonic nanostructure array. *Opt. Express* **2016**, *24*, 20613−20620.
(60) Byram, C.; Moram, S. S. B.; Shaik, A. K.; Soma, V. R. Versatile gold based SERS substrates fabricated by ultrafast laser ablation for sensing picric acid and ammonium nitrate. *Chem. Phys. Lett.* **2017**, *685*, 103−107.
(61) Tripathi, A.; Emmons, E. D.; Kline, N. D.; Christesen, S. D.; Fountain, A. W., III; Guicheteau, J. A. Molecular structure and solvent factors influencing SERS on planar gold substrates. *J. Phys. Chem. C* **2018**, *122*, 10205−10216.
(62) Pilot, R.; Signorini, R.; Durante, C.; Orian, L.; Bhamidipati, M.; Fabris, L. A review on surface-enhanced Raman scattering. *Biosensors* **2019**, *9*, 57.
(63) Fountain, A. W.; Christesen, S. D.; Moon, R. P.; Guicheteau, J. A.; Emmons, E. D. Recent advances and remaining challenges for the

https://doi.org/10.1021/acsomega.2c01095
ACS Omega 2022, 7, 15969−15981

spectroscopic detection of explosive threats. *Appl. Spectrosc.* **2014**, *68*, 795−811.
(64) Zrimsek, A. B.; Wong, N. L.; Van Duyne, R. P. Single molecule surface-enhanced Raman spectroscopy: a critical analysis of the bianalyte versus isotopologue proof. *J. Phys. Chem. C* **2016**, *120*, 5133−5142.
(65) Schlücker, S. Surface-Enhanced raman spectroscopy: Concepts and chemical applications. *Angew. Chem., Int. Ed.* **2014**, *53*, 4756−4795.
(66) Akinoglu, G. E.; Akinoglu, E. M.; Kempa, K.; Hutchison, J. A. Materials design of vertically coupled plasmonic arrays. *Nanocale* **2021**, *3*, 6925.

https://doi.org/10.1021/acsomega.2c01095
ACS Omega 2022, 7, 15969−15981